4116 *Biochemistry* **2010,** *49,* 4116–4125
DOI: 10.1021/bi100102s

BIOCHEMISTRY
including biophysical chemistry & molecular biology
Article

Substitution of Ala for Tyr567 in RB69 DNA Polymerase Allows dAMP To Be Inserted opposite 7,8-Dihydro-8-oxoguanine[†,‡]

Jeff Beckman,[§] Mina Wang,[§] Gregor Blaha, Jimin Wang,* and William H. Konigsberg*

Department of Molecular Biophysics and Biochemistry, Yale University, New Haven, Connecticut 06520-8024.
[§]These authors contributed equally to this work.

Received January 22, 2010; Revised Manuscript Received March 3, 2010

ABSTRACT: Accurate copying of the genome by DNA polymerases is challenging due in part to the continuous damage inflicted on DNA, which results from its contact with reactive oxygen species (ROS), producing lesions such as 7,8-dihydro-8-oxoguanine (8-oxoG). The deleterious effects of 8-oxoG can be attributed to its dual coding potential that leads to G → T transversions. The wild-type (wt) pol α family DNA polymerase from bacteriophage RB69 (RB69pol) prefers to insert dCMP as opposed to dAMP when situated opposite 8-oxoG by > 2 orders of magnitude as demonstrated using pre-steady-state kinetics ($k_{pol}/K_{d,app}$). In contrast, the Y567A mutant of RB69pol inserts both dCMP and dAMP opposite 8-oxoG rapidly and with equal efficiency. We have determined the structures of preinsertion complexes for the Y567A mutant with dATP and dCTP opposite a templating 8-oxoG in a 13/18mer primer-template (P/T) at resolutions of 2.3 and 2.1 Å, respectively. Our structures show that the 8-oxoG residue is in the *anti* conformation when paired opposite dCTP, but it flips to a *syn* conformation forming a Hoogstein base pair with an incoming dATP. Although the Y567A substitution does not significantly change the volume of the pocket occupied by *anti*-8-oxoG, it does provide residue G568 the flexibility to move deeper into the minor groove of the P/T to accommodate, and stabilize, *syn*-8-oxoG. These results support the hypothesis that it is the flexibility of the nascent base pair binding pocket (NBP) in the Y567A mutant that allows efficient insertion of dAMP opposite 8-oxoG.

DNA polymerases ensure accurate replication of genomic DNA, making errors only once in every 10^3−10^6 insertion events. When available, intrinsic exonuclease activity in the same polypeptide chain decreases the error rate by an additional 100-fold. Extrinsic exonucleases, nucleotide base excision repair, and mismatch repair systems (NER, BER, and MMR) further increase replication fidelity. Overall, the combined effects of these systems lead to only one error per 10^{9-10} base pairs polymerized (*1*, *2*).

7,8-Dihydro-8-oxoguanine (8-oxoG)[1] is a common DNA base adduct that has high mutagenic potential (*3*, *4*). It has been estimated that approximately 100−400 of these adducts are formed within a mammalian cell per day (*5*). Reactive oxygen species (ROS), such as the hydroxyl radical ·OH, directly attack the C-8 position of guanine (*3*). This adduct, which is simply guanine with a C-8 carbonyl oxygen (O-8), has the potential to form two hydrogen bonds with dATP when 8-oxoG flips from an *anti* to a *syn* conformation (Figure 1), making it an acceptable template for dATP as well as dCTP, resulting in G → T transversions that have been linked to cancer and other diseases (*6*, *7*).

DNA polymerases vary widely in their ability to select against insertion of dAMP opposite 8-oxoG, even within the same polymerase family. It has been shown that most A family pols, such as KF, pol II, and T7, preferentially insert dCMP opposite 8-oxoG, whereas pol BF, an A family DNA pol from *Bacillus stearothermophilus*, prefers to insert dAMP versus dCMP by 10-fold (*8*−*11*). Beese et al. (*8*) have shown that the ability of BF to preferentially insert dAMP relative to dCMP opposite 8-oxoG was likely due, in part, to the formation of a hydrogen bond between O-8 of *syn*-8-oxoG and an amide hydrogen of Q797, in addition to the two interbase hydrogen bonds (*8*). In contrast, Ellenberger et al. showed that T7 pol lowers the efficiency of dAMP insertion relative to dCMP opposite *syn*-8-oxoG because of an unfavorable steric and/or electrostatic interaction between N-2 of *syn*-8-oxoG and the protonated primary amine of K536 (*11*, *12*). DNA polymerases from the B family, such as RB69pol, human pol α, calf thymus pol δ, and the DNA pol from bacteriophage φ29 (φ29pol), vary widely in their ability to insert

[†]This work was supported by U.S. Public Health Service Grant GM063276-05.

[‡]With regard to author contributions, J.B. determined the kinetic parameters, M.W. crystallized and determined the structures of RB69pol−8-oxoG ternary complexes, G.B. collected data at NSLS (Brookhaven), and J.B., J.W., and W.H.K. helped to interpret the data, designed experiments, and contributed to writing the paper.

*To whom correspondence should be addressed. J.W. or W.H.K.: Department of Molecular Biophysics and Biochemistry, Yale University, 333 Cedar St., SHM CE-14, New Haven, CT 06520-8024; telephone, (203) 785-4599; fax, (203) 785-7979; e-mail, jimin.wang@yale.edu (J.W.) or william.konigsberg@yale.edu (W.H.K.).

[1]Abbreviations: 8-oxoG, 7,8-dihydro-8-oxoguanine; pols, DNA polymerases; wt, wild-type RB69pol; RB69pol, bacteriophage RB69 DNA polymerase; NBP, nascent base pair binding pocket; 3DA, 3-deazaadenine; dAP, 2-aminopurine; I, hypoxanthine; Pu, purine; Py, pyrimidine; Cα-H, methylene hydrogen atom of Gly; dNMP, deoxynucleoside monophosphate; dNTP, deoxynucleoside triphosphate; k_{obs}, observed rate constant; k_{pol}, maximum rate of dNMP insertion; $K_{d,app}$, dNTP concentration that supports the half-maximal rate of dNMP insertion; PCNA, proliferating cell nuclear antigen; T7, DNA polymerase from T7 bacteriophage; KF, Klenow fragment of *Escherichia coli* DNA polymerase I; pol II, *E. coli* DNA polymerase II; PDB, Protein Data Bank; rmsd, root-mean-square deviation.

 Published on Web 04/22/2010

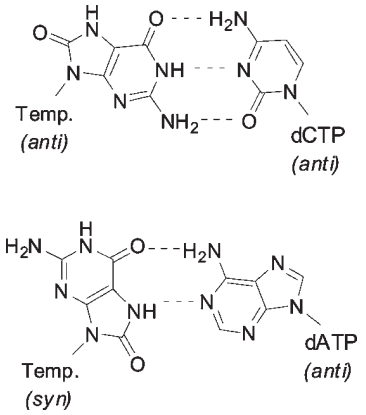

FIGURE 1: Structures of an incoming dCTP or dATP paired opposite a templating 8-oxoG. 8-oxoG likely flips into the *syn* conformation to pair opposite dATP to form a base pair comparable to the dATP·T base pair, with two interbase hydrogen bonds.

dAMP relative to dCMP opposite 8-oxoG (*13*−*16*). For example, human pol α was recently shown to favor dATP, although both were inserted with very low efficiency (*13*), but calf thymus pol δ, in the presence of PCNA, favors dCTP by several-fold (*14*).

RB69pol was previously found to discriminate against dAMP relative to dCMP opposite 8-oxoG (*15*). Modeling studies have suggested that the low efficiency of insertion of dAMP opposite 8-oxoG by wt RB69pol was due to a steric clash between *syn*-8-oxoG and residue G568 (*15*), although the authors suggested that the adjacent Y567 residue was helping to create a steric environment for G568, thereby indirectly causing destabilization of *syn*-8-oxoG (*15*). Steady-state kinetic analysis of the Y390S replacement in ϕ29pol (the equivalent of Y567 in RB69pol) showed a decrease in the level of discrimination for insertion of dAMP relative to dCMP opposite 8-oxoG, lending support to this conclusion (*16*). Modeling studies have suggested that the equivalent tyrosine residue in DNA pols of other families, e.g., Y955 and Y530 of the family A DNA pols human pol γ and T7 pol, respectively, and Y271 of the family X human pol β, would also act as steric blocks for insertion of dAMP opposite 8-oxoG (*11*, *17*−*19*), and it had been found that the human pol γ Y955C mutant reduced the level of discrimination of dAMP opposite 8-oxoG in a manner similar to that of the ϕ29pol Y390S mutant (*16*, *19*). Interestingly, the pol γ Y955C mutant was discovered while patients suffering from progressive external ophthalmoplegia (PEO) were being screened, suggesting a link between dementia and oxidative stress (*19*).

To test if Y567 in RB69pol modulates the insertion of dAMP opposite 8-oxoG, we compared the pre-steady-state kinetic parameters for insertion of dAMP and dCMP opposite 8-oxoG by wt RB69pol, and its Y567A and L561A mutants. We included the RB69pol L561A mutant because its side chain is close to the templating base (Figure 2), and replacing Leu with the much smaller Ala would be expected to allow 8-oxoG more freedom to "sample" alternative conformations upon binding of an incoming dATP. We found that the Y567A mutant increased the rate of insertion of dAMP opposite 8-oxoG by almost 3 orders of magnitude relative to that of wt RB69pol, but the L561A mutant did not. To understand why wt was so restrictive and Y567A so permissive, we determined crystal structures of the preinsertion ternary complexes of the Y567A mutant with dCTP and dATP opposite a templating 8-oxoG (at 2.1 and 2.3 Å resolution, respectively). When we compared these structures with those of the wt·dCTP·8-oxoG and wt·dTTP·A ternary complexes

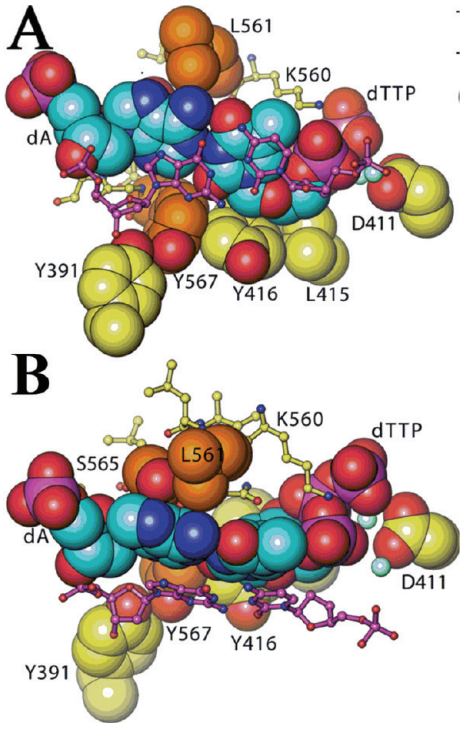

FIGURE 2: Steric relationship of some of the NBP residues surrounding an incoming dTTP paired opposite a templating A (from ref *20*, PDB entry 1IG9). (A) The nascent base pair and surrounding residues are shown from the duplex side of the primer-template in space-filling form [the terminal base pair is shown in stick form (purple) for the sake of clarity]. L561 and Y567 are colored orange. (B) Orthogonal view of panel A, showing the proximity of L561 with the templating base.

obtained previously (*15*, *20*), we were able to rationalize the kinetic behavior of the wt and the Y567A mutant in structural terms as described below.

EXPERIMENTAL PROCEDURES

Materials. Materials and reagents were of the highest quality commercially available. dNTPs were purchased from Roche (Burgess Hill, U.K.). T4 polynucleotide kinase was purchased from New England Biolabs (Ipswich, MA), and [γ-^{32}P]ATP was purchased from MP Biomedicals (Irvine, CA). d(3DA)TP was generously provided by R. D. Kuchta (University of Colorado, Boulder, CO).

Enzymes. Wild-type RB69pol and the Y567A and L561A mutants in the exonuclease-deficient background (D222A and D327A) were overexpressed in *Escherichia coli*, purified, and stored as previously described (*21*).

DNA Substrates. Sequences of primer-templates (P/T) used in this study are shown in Table 1. Oligonucleotides were synthesized at the Keck facilities (Yale University). Primers were labeled on the 5′-end with ^{32}P using T4 polynucleotide kinase and [γ-^{32}P]ATP (except when used for crystallography) and annealed to unlabeled templates as previously described (*22*, *23*).

Chemical Quench Experiments. Experiments were performed at 23 °C with a buffer solution of 66 mM Tris-HCl (pH 7.4). Rapid chemical quench experiments were conducted using the KinTek rapid quench instrument (Model RQF-3, KinTek Corp., University Park, PA). For k_{pol} and $K_{d,app}$ determinations, experiments were performed under single-turnover conditions, with a 10-fold excess of RB69pol over P/T. Although this large excess of RB69pol over P/T should ensure

Table 1: Primer-Template Sequences Used in This Study[a]

GCGGACTGCTTAC GCGCCTGACGAATG**G**ACT	D_G
GCGGACTGCTTAC GCGCCTGACGAATG**G**$_o$ACT	D_{OG}
GCGGACTGCTTAC^{-dd} GCGCCTGACGAATG**G**$_o$ACT	D_{OG}^{dd}
GCGGACTGCTTACC GCGCCTGACGAATGG$_o$**A**CT	$D_{C:OG}$
GCGGACTGCTTACA GCGCCTGACGAATGG$_o$**A**CT	$D_{A:OG}$
GCGGACTGCTTAC GCGCCTGACGAATG**A**TCT	D_A
GCGGACTGCTTAC GCGCCTGACGAATG**A**$_{3D}$TCT	D_{3DA}

[a]The templating base is in bold. G_o is 8-oxoG, and A_{3D} is 3-deazaadenine (3DA). D_{OG}^{dd} was used to grow the crystal structures discussed.

single turnover, the condition for this to occur is that all of the P/T binds productively to RB69pol. This condition is not always met, as we had discovered previously with the RB69pol "triple mutant" L561A/S565G/Y567A (*24*). To ensure that single-turnover conditions were obeyed, we added heparin (final concentration of 1 mg/mL) to trap any enzyme that was released from the P/T. In some instances, the heparin trap could not be used because the rate of product formation was too low to obtain accurate kinetic parameters, e.g., insertion of dAMP opposite 8-oxoG by wt. Briefly, enzyme and P/T from one syringe were rapidly mixed with Mg^{2+}, heparin, and various dNTP concentrations from the other syringe for times ranging from 5 ms to 1 min. For reactions that required longer times, experiments were performed manually on the benchtop. The final concentrations after mixing were as follows: 1 μM enzyme, 90 nM P/T, and 10 mM Mg^{2+}. Reaction mixtures were quenched with 0.5 M EDTA (pH 8.0). Substrates and products were separated by PAGE [19:1 (w/v) acrylamide:bisacrylamide gels containing 8 M urea], visualized using a STORM imager (Molecular Imaging), and quantified using Imagequant (GE Healthcare) and GraphPad Prism.

Data Analysis. The amount of product formed versus time for each dNTP concentration was fitted by nonlinear regression to the general form of eq 1 to yield observed rates of product formation, k_{obs}:

$$Y = \sum_{i=1}^{n} A_i e^{-k_i t} + C \quad (1)$$

where Y is the concentration of the DNA product formed during the reaction, C is the offset constant, A_i is the observed amplitude of product formation, and k_i is the observed rate constant. The kinetic parameters k_{pol} (the rate of phosphoryl transfer) and $K_{d,app}$ (defined as the dNTP concentration at which the rate of phosphoryl transfer reaches $^1/_2 k_{pol}$) were obtained by fitting plots of k_{obs} versus dNTP concentration to eq 2:

$$k_{obs} = \frac{k_{pol}[dNTP]}{K_{d,app} + [dNTP]} \quad (2)$$

Table 2: Pre-Steady-State Kinetic Parameters for the Insertion of dNMPs by Wild-Type RB69pol and Its Mutants

enzyme	dNTP	template	k_{pol} (s^{-1})	$K_{d,app}$ (μM)	$k_{pol}/K_{d,app}$ (μM^{-1} s^{-1})
wild type	dCTP	8-oxoG	55	97	0.57
	dATP	8-oxoG	1.7	1500	1.1×10^{-3}
L561A	dCTP	8-oxoG	76	11	6.9
	dATP	8-oxoG	9.5	980	9.7×10^{-3}
Y567A	dCTP	8-oxoG	91	29	3.1
	dATP	8-oxoG	110	48	2.3
	dGTP	A	0.015	250	6.0×10^{-5}[a]
	dITP	A	~0.50	~1000	5.0×10^{-4}[b]
	dGTP	dAP	~0.15	~200	8.0×10^{-4}[b]
	dITP	dAP	ND[c]	ND[c]	3.0×10^{-5}[d]

[a]Data obtained previously (*24*). [b]Values are estimates because the k_{obs} values decreased with an increasing dNTP concentration. $K_{d,app}$ and k_{pol} values in these cases were obtained by fitting k_{obs} vs dNTP concentration to eq 3. [c]Not determined because the value of $K_{d,app}$ was too high (> 2 mM). [d]The $k_{pol}/K_{d,app}$ second-order value was obtained in this case by calculating the slope of a linear line fitted to the data: $y = mx + b$, where m = the slope = $\Delta k_{obs}/\Delta[dNTP] = k_{pol}/K_{d,app}$. Of the values shown, standard deviations were 10−20 and ~30% for k_{pol} and $K_{d,app}$ values, respectively.

where k_{obs} represents the observed rate at a given dNTP concentration. Note that the $K_{d,app}$ values are not ground-state dissociation constants of dNTP binding. This is because the observed dNTP concentration dependence of rates of product formation are affected by "hidden" steps that occur subsequent to dNTP binding but prior to phosphoryl transfer, such as the step defining an induced-fit conformational change. Interestingly, insertion of d(hypoxanthine)TP (dITP) opposite A, and dGMP opposite dAP (2-aminopurine) (Table 2), resulted in k_{obs} values that decreased with an increasing dITP concentration, a situation similar to what Johnson et al. (*25*, *26*) found with AZT and d(8-oxoG)MP insertion opposite T and C, respectively, by the human mitochondrial DNA polymerase γ. [The complex kinetics may have been caused by a slow release of pyrophosphate subsequent to chemistry, thereby allowing pyrophosphorolysis to compete with phosphodiester bond formation (*26*).] Values of $K_{d,app}$ were estimated in these cases by fitting plots of k_{obs} versus dNTP concentration to eq 3:

$$k_{obs} = \frac{\Delta k_{obs}[dNTP]}{K_{d,app} + [dNTP]} \quad (3)$$

where Δk_{obs} is the overall change in the observed rate given the range of dNTP concentrations.

Crystallization of RB69pol Ternary Complexes. D_{OG}^{dd} was used for all crystallizations (Table 1). The primer was dideoxy-terminated at the 3′-end to prevent nucleotide insertion. The RB69pol Y567A mutant was mixed in an equimolar ratio with freshly annealed D_{OG}^{dd}. dCTP or dATP was then added to give a final concentration of 2.5 mM. For equilibration, using microbatch vapor-diffusion methods for crystallization, equal volumes of a well solution containing 150 mM $CaCl_2$, 14% (w/v) PEG 350 monomethyl ether (MME), and 100 mM sodium cacodylate (pH 6.5) were added to the RB69pol·D_{OG}^{dd}·dCTP mixture, and 150 mM $CaCl_2$, 11% (w/v) PEG 350 MME, and 100 mM sodium cacodylate (pH 6.5) were added to the RB69pol·D_{OG}^{dd}·dATP mixture. Crystals typically grew in 2−3 days at 20 °C. The square rod-shaped crystals had typical dimensions of 0.2 mm × 0.1 mm × 0.1 mm. Crystals were transferred from the mother liquor to a cryoprotectant/precipitant stabilization solution containing 20% (w/v) PEG 350 MME, 100 mM $CaCl_2$, and

Table 3: Data Collection and Refinement Statistics for Ternary Complexes

	dATP vs d-8-oxoG	dCTP vs d-8-oxoG
unit cell [*a*, *b*, *c* (Å)]	78.148, 117.603, 130.681	76.394, 121.089, 122.857
resolution range (highest-resolution shell) (Å)	50.0−2.30 (2.38−2.30)	38.81−2.05 (2.12−2.05)
no. of unique reflections	51799 (4177)	65594 (5020)
redundancy	4.2 (3.0)	3.8 (2.3)
completeness (%)	95.3	90.7
R_{merge}	8.3 (> 100)	7.3 (96.2)
signal-to-noise ratio ($\langle I/\delta I \rangle$)	15.3 (0.95)	16.5 (1.03)
model contents		
no. of amino acid residues	903	903
no. of water molecules	176	580
no. of Ca^{2+} ions	5	4
no. of template nucleotides	18	18
no. of primer nucleotides	13	13
no. of dNTP molecules	1	1
R (%)	20.56	20.99
R_{free} (%)	25.77	25.59
rmsd for bonds (Å)	0.0084	0.0092
rmsd for bond angles (°)	1.220	1.249

100 mM sodium cacodylate (pH 6.5). Crystals were then gradually transferred into a cryoprotectant/precipitant solution with the same components but with up to 30% (w/v) PEG 350 MME prior to freezing in liquid nitrogen.

Data Collection, Structure Determination, and Refinement. Crystals were first characterized using home radiation sources. X-ray diffraction data were collected using synchrotron radiation sources at beamline X29 at Brookhaven National Laboratory (NSLS, Upton, NY) at a wavelength of 1.075 Å and at 110 K. Crystals belonged to orthorhombic space group $P2_12_12_1$ with different unit cell parameters (Table 3). Data were integrated and scaled using the HKL2000 program suites (*27*).

Structures were determined using molecular replacement methods with AMORE (*28*), starting with the ternary complex structure of wild-type RB69pol (*20*), and refined using REFMAC5 (*29*). Using Coot (*30*), the DNA duplex and dNTP were built into the electron density maps phased by the partially refined polymerase model. We observed two Ca^{2+} ions occupying the A and B metal ion sites, which had been observed previously (*20*). Structure refinement statistics are summarized in Table 3. Figures obtained from the crystal structures were created using Ribbons (*31*).

PDB Entries. Coordinates and structure factors for the Y567A mutant dCTP·*anti*-8-oxoG and dATP·*syn*-8-oxoG ternary complex structures have been deposited in the Protein Data Bank as entries 3LZJ and 3LZI, respectively.

RESULTS

Insertion of dAMP Relative to dCMP opposite 8-oxoG by Wild-Type and Mutant RB69 pols. Steady-state kinetic analysis had previously shown that wt RB69pol inserted dCMP opposite 8-oxoG 20 times more efficiently than dAMP (*15*). We confirmed this result, but under pre-steady-state conditions; i.e., comparing $k_{pol}/K_{d,app}$ specificity constants, we found a 500-fold difference between the ability of wt to insert dCMP versus dAMP opposite 8-oxoG (Table 2). In theory, $k_{pol}/K_{d,app}$ should be equal to the steady-state approximation k_{cat}/K_m (*32*), but in our case, the pre-steady-state values differed from steady-state values. Figure 3A,B shows a representative set of data used to obtain k_{pol} and $K_{d,app}$ values when a dNMP is inserted opposite 8-oxoG in the presence of a heparin trap (see Experimental Procedures),

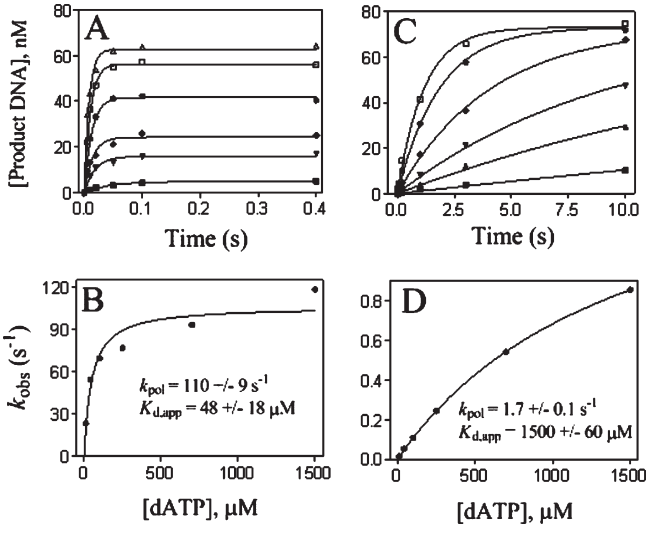

FIGURE 3: Kinetics of insertion of dAMP opposite 8-oxoG by the Y567A mutant (A and B) and the wt (C and D). (A) Progress curves at various dATP concentrations, 10, 40, 100, 250, 700, and 1500 μM (from bottom to top), fit to single-exponential equations. Heparin (1 mg/mL) was used to prevent rebinding of the enzyme to the P/T. (B) Plot of k_{obs} vs dATP concentration fit to eq 2 to yield k_{pol} and $K_{d,app}$. (C) Same as panel A but with the wt. Progress curves were obtained without a heparin trap. (D) Same as panel B using the results depicted in panel C.

in this case dAMP opposite 8-oxoG catalyzed by the Y567A mutant. No discernible "burst" of dAMP insertion opposite 8-oxoG by the wt was observed even at 500 μM dATP (data not shown), so kinetic parameters could be estimated only from data derived from progress curves representing multiple turnovers (without a heparin trap) (Figure 3C,D). In this case, the specificity constants k_{cat}/K_m and $k_{pol}/K_{d,app}$ are approximately equal because phosphoryl transfer was rate-limiting (*33*).

We wanted to find out which NBP residues serve as a barrier to insertion of dAMP opposite 8-oxoG. The crystal structure (*20*) of the wt RB69pol·D_A·dTTP complex showed that O helix residue L561, which is in the proximity of the adenine templating base (Figure 2B), could hinder the binding of *syn*-8-oxoG if it was the templating base instead of A. However, the level of discrimination against dAMP insertion by the L561A mutant remained as high as that of the wild type, with a 700-fold preference for

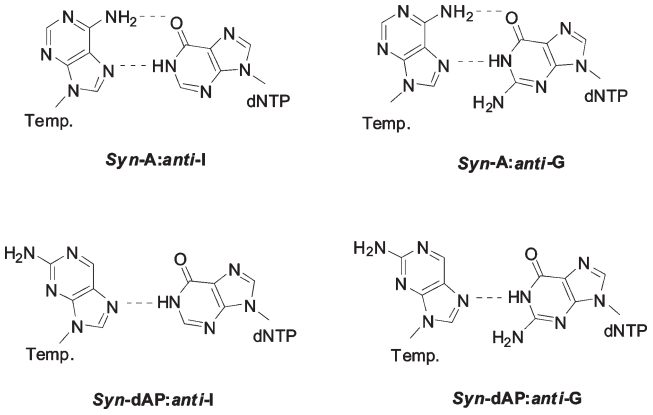

FIGURE 4: Purine·purine nascent base pairs poorly utilized by the Y567A mutant.

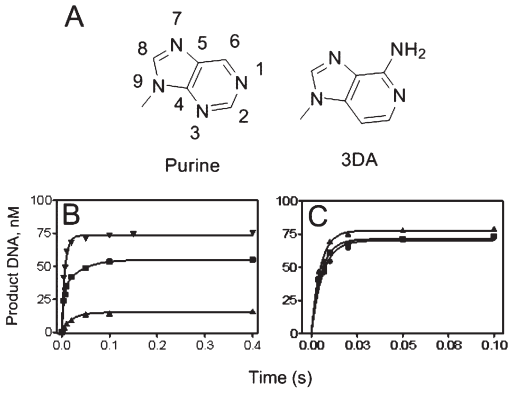

FIGURE 5: Progress curves for wt RB69pol and the Y567A mutant for insertion of d(3DA)MP opposite T and dTMP opposite 3DA. Data were obtained under single-turnover conditions with saturating [dNTP]s (see Experimental Procedures). (A) Shown are the purine numbering scheme (left) and 3-deazaadenine (3DA) (right). (B) Rate of DNA product formation for insertion of dTMP opposite 3DA by wt (▲), dTMP opposite A by wt (▼), and dTMP opposite 3DA by the Y567A mutant (■). (C) Rate of DNA product formation for insertion of d(3DA)TP opposite T by wt (■), dATP opposite T by wt (●), and dTMP opposite 3DA by the Y567A mutant (▲).

incorporation of dCMP over dAMP (Table 2). We also substituted Y567 with Ala, and we found that the Y567A mutant incorporated both dAMP and dCMP opposite 8-oxoG with equal efficiency, in contrast to the results obtained with L561A. The individual kinetic parameters were within 2- or 3-fold of the values obtained for insertion of dCMP opposite 8-oxoG by wt, so the Y567A mutant caused RB69pol to lose fidelity solely by having the ability to increase the efficiency of dAMP insertion (Table 2).

Can Other dNTP Derivatives That Form Nascent Pu—Pu Base Pairs, Such as Hypoxanthine (I)·A, Be Utilized for Primer Extension? Because the Y567A mutant did not discriminate against the formation of a dATP·*syn*-8-oxoG base pair, we wanted to find out if the Y567A mutant would utilize other nascent purine·purine base pairs, e.g., a dITP·dA base pair, with comparable efficiency. If negative results were obtained, one could argue that the dATP·*syn*-8-oxoG base pair presented a unique situation. We had previously shown that the Y567A mutant inefficiently inserted dGMP opposite dA, despite the fact that a dGTP·*syn*-A base pair could form two interbase hydrogen bonds, just like the dATP·*syn*-8-oxoG base pair (Figure 4 and Table 2) (*24*). To test if other Pu·Pu mispairs could be utilized by the Y567A mutant, we investigated the ability of the Y567A mutant to insert dIMP opposite A as well as dGMP and dIMP opposite dAP (Figure 4) and found very low levels of insertion (Table 2), suggesting that the Y567A mutant still retained some ability to discriminate against the formation of other Pu·Pu mispairs.

Can a dTTP·3DA Nascent Base Pair Be Used for Primer Extension by wt RB69pol or Its Y567A Mutant? Because insertion of dATP opposite 8-oxoG by the Y567A mutant was unique as being the only Pu·Pu mispair that could be efficiently utilized, there is likely to be some specific feature(s) of the templating 8-oxoG that the Y567A mutant recognizes to utilize dATP. Since 8-oxoG was the only purine base with a C-8 carbonyl oxygen that was tested, it seemed reasonable to assume that it could be a hydrogen bond acceptor of the Cα hydrogen atom (Cα-H) of residue G568 (*34*) which could firmly anchor the templating 8-oxoG and enhance the rate of phosphoryl transfer. By analogy, N-3 of a templating purine in the *anti* conformation may also be a H-bond acceptor of the Cα-H of G568, because of the proximity of G568 and templating purines in the RB69pol ternary structures (*15*, *20*). Assuming that a Cα-H···N hydrogen bond could help to stabilize a nascent pyrimidine·purine (py·pu) base pair, removing N-3 from a templating dA and replacing it with C-H [forming 3DA (Figure 5A)] would be expected to cause destabilization of the nascent base pair, leading to a less efficient insertion of the "correct" dNMP. Insertion of dTMP opposite a templating 3DA, by the wt and the Y567A mutant, resulted in progress curves with a significant reduction in efficiency, relative to insertion of dTMP opposite A (Figure 5B). In contrast, the reciprocal situation of inserting d(3DA)MP opposite T by either wt or the Y567A mutant resulted in k_{pol} values and amplitudes comparable to those obtained when dAMP was inserted opposite T (Figure 5C).

Extention past C·8-oxoG and A·8-oxoG Base Pairs. Bypass of base pairs containing 8-oxoG as the templating base was very inefficient with wt RB69pol (Table 4). The main effect of having an 8-oxoG in the penultimate position 3′ to the templating base was to increase the $K_{d,app}$ for correct incoming dNTPs, by at least 2 orders of magnitude relative to the situation in which extension occurs with a normal P/T that does not have an 8-oxoG lesion (Table 4). With the wt, the $K_{d,app}$ values were too high (>2 mM) for an accurate determination of k_{pol}, but it was apparent that extrapolation of the plots of k_{obs} versus dTTP concentration (the next correct dNTP) would give higher k_{pol} and $K_{d,app}$ values for insertion past an A·8-oxoG base pair, relative to insertion past a C·8-oxoG base pair, resulting in approximately equal efficiencies for insertion of dTMP opposite A when bypassing A·8-oxoG and C·8-oxoG base pairs (Figure 6). This result concurs with a previous report by Kisker et al. (*15*). In contrast, the Y567A mutant bypassed both A·8-oxoG and C·8-oxoG base pairs much more efficiently, with $k_{pol}/K_{d,app}$ values 20- and 60-fold higher than with wt, respectively.

Crystal Structures of the Y567A Mutant in a Complex with a Dideoxy Primer-Template Containing a Templating 8-oxoG opposite dATP or dCTP. To correlate the kinetic results with the RB69pol structure, it was necessary to obtain high-quality crystals of the various complexes under study. Crystal structures of wt RB69pol ternary complexes containing a templating 8-oxoG and an incoming dCTP have already been reported (*15*), but there was no information about ternary complexes of the RB69pol Y567A mutant with P/Ts having a templating 8-oxoG opposite dCTP and dATP. To fill this gap, we were able to determine crystal structures of the ternary complexes

Table 4: Kinetic Parameters for Insertion of Correct dNMPs past C·8oxoG and A·8oxoG Terminal Base Pairs

		wt RB69pol			Y567A		
dNTP	P/T	k_{pol} (s^{-1})	$K_{d,app}$ (μM)	$k_{pol}/K_{d,app}$ (μM^{-1} s^{-1})	k_{pol} (s^{-1})	$K_{d,app}$ (μM)	$k_{pol}/K_{d,app}$ (μM^{-1} s^{-1})
dTTP	$D_{C\cdot OG}$	ND[a]	ND[a]	0.0050[b]	230	740	0.31
	$D_{A\cdot OG}$	ND[a]	ND[a]	0.012[b]	200	850	0.24

[a]Not determined because $K_{d,app}$ values were too high (>2 mM) (see Figure 6). [b]See footnote d from Table 2. Data from Figure 6 were fitted to a linear equation to yield $k_{pol}/K_{d,app}$. Standard deviations were within the same range as the data presented in Table 2.

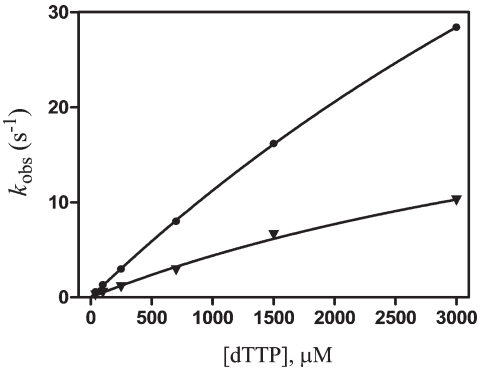

FIGURE 6: k_{obs} vs dTTP concentration plots of wt RB69pol extending primers beyond A·8-oxoG (●) and C·8-oxoG (▼) terminal base pairs.

mentioned above, at 2.1 and 2.3 Å resolution, respectively. The structures were well-refined, with R_{free} values of ~25 (Table 3). Note that calcium ions were used as the metal ion cofactor to crystallize these complexes, instead of magnesium. Unlike magnesium, the cofactor that brings about rapid phosphoryl transfer, calcium did not lead to phosphoryl transfer, even in the presence of the 3′-OH (which was absent in these structures), so it is very likely that these structures represent inactive complexes. However, the goal here was to obtain new insights into base selectivity by (i) determining the precise interactions between the incoming dNTP and 8-oxoG, (ii) determining the location and geometry of the nascent base pair with respect to residues in the NBP, and (iii) comparing these structures with those from previous studies that used virtually identical conditions to crystallize RB69pol (*15*, *20*). With the Y567A mutant·dCTP·8-oxoG structure, we observed three hydrogen bonds between the incoming dCTP and 8-oxoG, with the 8-oxoG oriented in the *anti* conformation (Figure 7A). When we superimposed the palm domains of the wt·dCTP·*anti*-8-oxoG structure (*15*) and the Y567A mutant·dCTP·*anti*-8-oxoG structure, there was an ~0.7 Å shift of the A567 and G568 residues laterally toward the Y416 side chain, relative to the wt, while approximately the same distance between the Cα-H of G568 and N-3 of *anti*-8-oxoG was maintained (Figure 8). The shift of these residues also permitted the nascent base pair to move in the same direction, presumably helping it to alleviate some strain between the 2′-deoxyribose 5′-carbon and O-8 of *anti*-8-oxoG (represented by circular arrows in Figure 8). Such a shift would be unlikely to occur in the wt RB69pol because of the Y567 side chain, which is hydrogen bonded to the side chain of Y391 and packed against the side chain of Y416, creating considerable rigidity in this region.

From the omit $F_o - F_c$ electron density maps of the two Y567A mutant ternary structures, we can see that the templating 8-oxoG adopts a *syn* conformation when it pairs with dATP, with

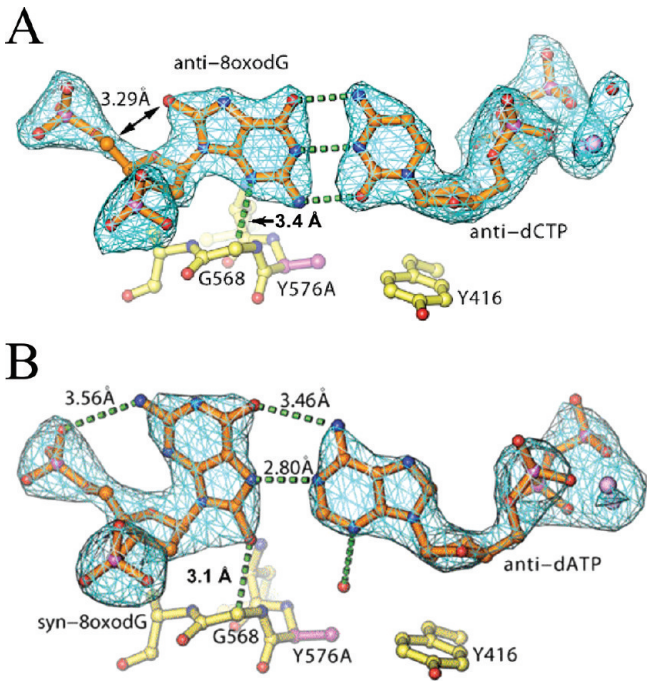

FIGURE 7: Crystal structures of the RB69pol Y567A mutant in a complex with *anti*-8-oxoG·dCTP and *syn*-8-oxoG·dATP base pairs. (A) Omitted $F_o - F_c$ electron density map of the *anti*-8-oxoG·dCTP nascent base pair. (B) Omitted $F_o - F_c$ electron density map of the *syn*-8-oxoG·dATP nascent base pair.

two interbase hydrogen bonds helping to stabilize it in the *syn* orientation in a manner analogous to that found with the A family DNA pols, BF pol and T7 pol (*8*, *12*) (Figure 7B). In addition, G568 was in the proximity of *syn*-8-oxoG so that an H-bond could form with the Cα-H of G568 and O-8 of *syn*-8-oxoG (interatom distance of 3.1 Å) (Figure 7B). Superimposing the palm domains of the Y567A mutant·dCTP·*anti*-8-oxoG structure with the corresponding Y567A mutant·dATP·*syn*-8-oxoG complex revealed that residues A567, G568, and A569 in the immediate vicinity of the Y567A mutation shifted toward Y416. There were no other significant changes (for example, L561, I570, and Y416 remained fixed) (Figure 9). Interestingly, the C-1′−C-1′ distance of the *anti*-dATP·*syn*-8-oxoG base pair, often used as a measure of base pair size, was 10.2 Å, which is shorter than that of the typical purine·pyrimidine base pair (10.6 Å).

DISCUSSION

It has been estimated that reactive oxygen species (ROS), e.g., ·OH, produce 100−400 8-oxoG residues per day per mammalian cell (*5*). The presence of 8-oxoG residues in DNA has been implicated in numerous diseases, including cancer (*35*, *36*), presumably because of its dual coding potential that leads to G → T tranversions. To help counter the dire effects of ROS

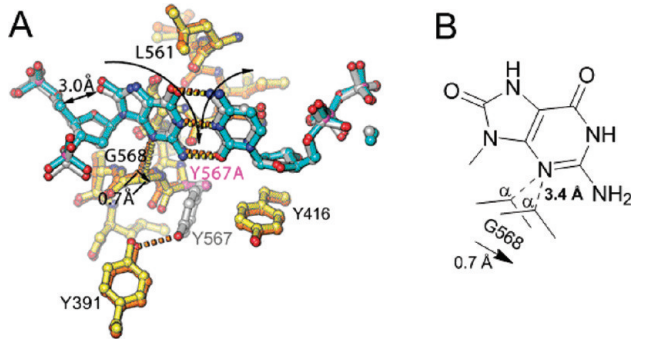

FIGURE 8: Comparison of the crystal structures of wt and the Y567A mutant in a complex with an *anti*-8-oxoG·dCTP base pair (*14*). (A) Superimposed palm domains showing that the Y567A substitution resulted in a shift of G568 by ~0.7 Å laterally toward Y416, relative to wt. Residues of the Y567A mutant and wt are colored yellow and orange, respectively, and the individual residues Y567 and Y567A are colored gray and magenta, respectively. The nascent base pairs in the wt and Y567A mutant structures are colored silver and blue, respectively. (B) Schematic illustration of the spatial relationship between G568 and the nascent base pair as shown in panel A.

mediated mutations, it is important to understand how human DNA polymerases insert dAMP opposite 8-oxoG. Because of the similarity between human DNA pols α and δ and RB69pol, the latter can serve as a good model for the human pols.

Several reports have proposed that the two hydrogen bonds formed between dATP and *syn*-8-oxoG (Figure 1) are partially responsible for its efficient utilization (*4*, *6*, *37*). Crystal and NMR structural studies of dATP·*syn*-8-oxoG base pairs within a DNA duplex show that they are compatible with B-form DNA, and their T_m values confirm that DNA duplexes containing these base pairs are at least as stable as those that do not (*38*−*40*). However, residues within the NBP, such as G568 of RB69pol, can alter the stability of this base pair, which could affect insertion of dAMP opposite 8-oxoG (*8*, *12*, *15*). On the basis of a comparison of the structures of a wt RB69pol·P/T binary complex containing an abasic site and a ternary complex containing a dCTP·*anti*-8-oxoG base pair, it was argued that G568 becomes "strained" upon binding of a template base into the polymerase NBP because the templating base would have to protrude into the minor groove of the DNA substrate by 1.9 Å (*15*). To explain the lower efficiency of insertion of dAMP opposite 8-oxoG by wt RB69pol, it was proposed that *syn*-8-oxoG would cause G568 to become even more strained by forcing it further into the minor groove of the DNA (*15*). Because the Y567A mutant increases the level of misinsertion (*41*), Kisker et al. (*15*) speculated that the Y567A substitution would relieve the strain imposed on G568 by providing some "wiggle room" in the NBP. The superimposed structures of the wt and the Y567A mutant in complexes with a dCTP·*anti*-8-oxoG base pair support this idea by showing that (i) the Y567A substitution causes G568 to shift by ~0.7 Å toward the space formerly occupied by the phenyl ring of Y567 (Figure 8) and (ii) the efficiency of insertion of dCMP opposite 8-oxoG ($k_{pol}/K_{d,app}$) increases 5-fold compared to that of the wt (Table 2).

Comparison of the Y567A·*anti*-8-oxoG·dCTP structure with the Y567A·*syn*-8-oxoG:dATP structure shows that G568 recedes into the DNA minor groove by ~0.6 Å (Figure 9), suggesting that the Y567A mutant provides G568 enough flexibility so that *syn*-8-oxoG can be easily accommodated. However, if G568 "strains" when packed against *syn*-8-oxoG, we would have expected a drop in relative efficiency of insertion of dAMP versus dCMP opposite 8-oxoG. Since this did not

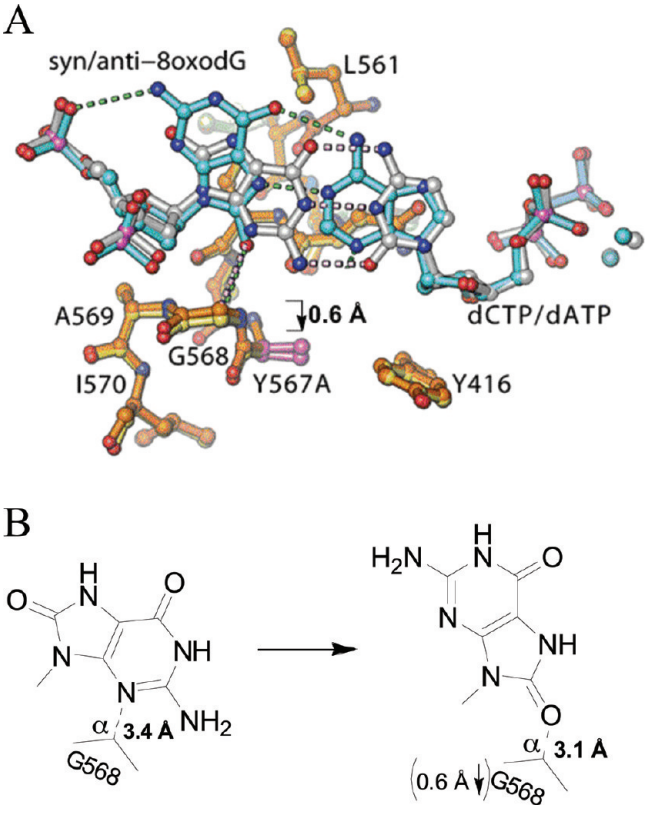

FIGURE 9: Comparison of the Y567A mutant·*anti*-8-oxoG·dCTP and Y567A mutant·*syn*-8-oxoG·dATP ternary crystal structures. (A) Superimposed palm domains showing that 8-oxoG flips from an *anti* to a *syn* conformation, resulting in a shift of A567 and G568 into the minor groove of the primer-template by ~0.6 Å. The Y567A·*anti*-8-oxoG·dCTP backbone is colored orange, and the Y567A·*syn*-8-oxoG·dATP backbone is colored yellow. (B) Schematic illustration of the spatial interaction between G568 and the nascent base pair as shown in panel A.

occur, G568 may not be strained after all. In fact, relative to the wt, the Cα-H of G568 is closer to O-8 of *syn*-8-oxoG (3.1 Å) (Figure 7B) in the Y567A mutant than to N-3 of *anti*-8-oxoG (3.4 Å) (Figure 7A). These findings, and our results with nucleotide analogues (vide supra), suggest that G568 provides additional stability to a nascent base pair, containing a templating 8-oxoG, by G568 donating its Cα-H to O-8 of *syn*-8-oxoG, or to N-3 of *anti*-8-oxoG. Previous studies with transmembrane proteins have shown that hydrogen bonds can form between Cα hydrogens of glycine and backbone carbonyl oxygens, i.e., Cα-H···O=C, stabilizing helical structures that transverse the lipid bilayer (*34*). These H-bonds provide ~3 kcal/mol if they are at an interatom distance of 3.0 Å, which is approximately the distance between *syn*-8-oxoG and G568 (Figure 7B). This is half the strength of an N···H-O hydrogen bond when it is in a hydrophobic environment like the NBP (*42*, *43*). The finding that the purine analogue 3DA (in which N-3 is replaced with C-H and thus cannot interact with G568) caused a significant reduction in the level of insertion of dTMP opposite 8-oxoG supports the notion that a Cα-H···N bond helps to stabilize this Pu·Py base pair as well (Figure 5B). Because this latter finding also applies to Watson−Crick base pairs, the stability of a nascent base pair may not be fully optimized via formation of interbase hydrogen bonds and/or by fitting snugly inside the NBP.

The finding that the Y567A substitution did not appreciably expand the NBP pocket in the vicinity of templating 8-oxoG in a manner that would relieve a steric clash until 8-oxoG flipped into

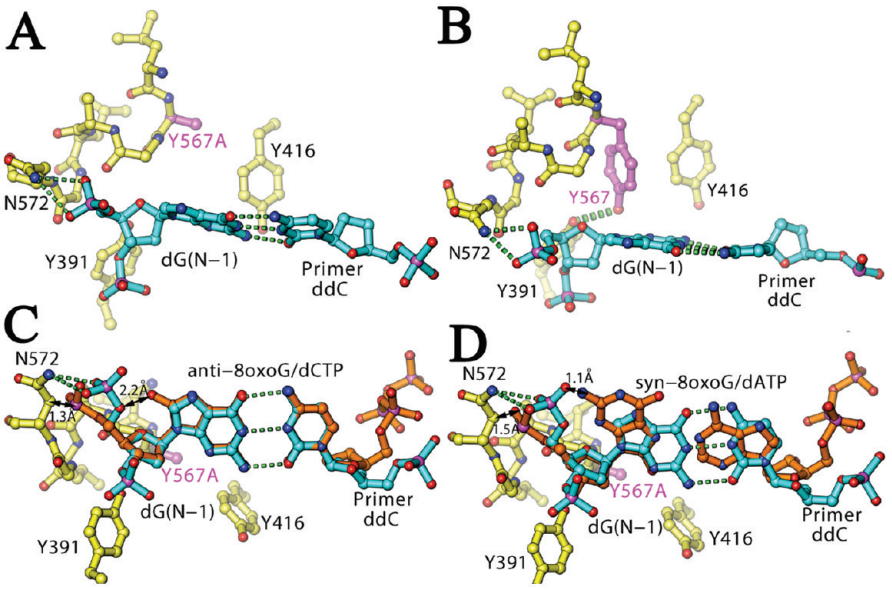

FIGURE 10: Computer modeling of the wt and the Y567A mutant ternary complex with the observed dATP·8-oxoG or dCTP·8oxoG base pair translocating from the nascent base pairing position to the product position. (A) Structure showing the terminal template base G [dG(N-1)] opposite the dideoxy-terminated nucleotide dC in the wt RB69pol ternary complex structure with Y567A modeled into the structure (PDB entry 1IG9). The mutation site is colored magenta. Hydrogen bonds are represented as green dotted lines. (B) Corresponding wt structure showing that Y567 and Y391 can form a hydrogen bond. (C) Superposition of the *anti*-8-oxoG·dCTP base pair onto the dG(N-1)·dC base pair. Black arrows denote unfavorable interactions. (D) Superposition of the *syn*-8-oxoG·dATP base pair onto the dG(N-1)·dC base pair. Black arrows denote unfavorable interactions.

a *syn* conformation (compare the schematics of Figures 8B and 9B) suggests that the Y567A mutant allows efficient insertion of dAMP opposite 8-oxoG by allowing G568 to have more flexibility (Figure 8A). Our previous analysis of RB69pol NBP mutants demonstrated that a larger NBP volume did not affect the rates of correct dNMP insertion but did give higher rates of misinsertion (*24*). The data presented here concur with this, by demonstrating that an expansion of the NBP leads to a higher efficiency of insertion of dAMP opposite 8-oxoG, without appreciably altering the kinetic parameters of insertion of dCMP opposite 8-oxoG. However, because dAMP is inserted opposite 8-oxoG more efficiently by the Y567A mutant than by the wt, because of a more flexible NBP, we argue that misinsertion occurs not only when steric clashes are removed but also when NBP residues fail to provide the interactions necessary to keep the pocket rigid.

Once inserted, a terminal base pair containing a templating 8-oxoG dramatically reduces the level of primer extension by the next correct incoming dNTP. Interestingly, bypass of a C·8-oxoG base pair by wt RB69pol occurs just as efficiently as the bypass of an A·8-oxoG base pair (Table 4), in contrast to what has been reported for all other DNA pols that more readily bypass a terminal A·8-oxoG base pair (e.g., refs *9*, *14*, and *44*) except for pol η (*45*). Superposition of the nascent base pairs of our RB69pol Y567A·*anti*-8-oxoG·dCTP or Y567A·*syn*-8-oxoG·dATP structures onto the terminal dG·dC base pair from the structure of the first RB69pol ternary complex determined (*20*) (Figure 10) provides new insights into the postchemistry translocation event and primer extension beyond the 8-oxoG base pair, namely that when the terminal 8-oxoG base pair fits into the cavity of wt RB69pol (within the active site), regardless of its conformation (*syn*-8-oxoG or *anti*-8-oxoG), 8-oxoG clashes into its own 5′-bridging phosphate or this phosphate clashes into the main chain backbone (N572, which itself donates two hydrogen bonds to the phosphate backbone) to avoid a steric clash with 8-oxoG. Specifically, if the 5′-bridging phosphate assumes the canonical conformation of the templating nucleotide residue (colored blue in Figure 10C,D), there would be a severe steric clash with O-8 of *anti*-8-oxoG or N-2 of *syn*-8-oxoG (Figure 10C,D). Thus, translocation must be coupled with a reorientation of the phosphate backbone of the templating nucleotide residues, and this explains why insertion of the next dNMP proceeds very slowly (Table 4). The modeling also suggests that the width of the binding pocket for the (N-1) base pair is too small for the 8-oxoG base pair to fit into the space provided by RB69pol. However, it appears that the 3′-OH of the new priming nucleotide residue is still in optimal alignment to facilitate rapid catalysis, suggesting that there are likely some differences between our modeling results and what occurs on the phosphoryl transfer pathway. We are in the process of obtaining the relevant crystal structures to identify these differences.

As with the wt, the precise structural features that allow the Y567A mutant to increase the level of extension of a primer beyond a terminal 8-oxoG base pair in the duplex cannot be identified without the relevant ternary crystal structures. However, on the basis of what is known about the kinetic and structural consequences regarding the flexibility that occurs with G568 in the Y567A mutant, we can anticipate that a similar situation might occur with respect to the binding pocket of the terminal base pair in the DNA duplex. Because the hydrogen bond between Y567 and Y391 in the wt likely provides rigidity for the NBP (Figure 10B), its absence should increase the flexibility of the local structures supporting the terminal base pair of the P/T, thus making it possible to accommodate terminal dN·8-oxoG base pairs. In addition, the increased flexibility due to the Y567A substitution may allow the base pair containing 8-oxoG to recede further into the minor groove.

Despite the sequence similarity between pols of the B family (*46*), the efficiency of insertion of dAMP and dCMP opposite 8-oxoG

varies considerably (*13*−*15*). However, conserved NBP residues, namely Y567 (using the RB69pol numbering scheme), would be expected to have similar roles in modulating dNMP insertion by these DNA pols, as well as by DNA pols from other families. Y567 is part of the highly conserved DNA polymerase motif B (*47*), and previous studies have used modeling of the preinsertion ternary complexes of DNA polymerases which have an *anti*-dCTP·*anti*-8-oxoG nascent base pair to show that the tyrosine residues corresponding to Y567 of RB69pol, namely, Y390 of ϕ29pol, Y530 of T7 DNApol, Y955 of human pol γ, and Y271 of human pol β, likely "block" the stable formation of an A·8-oxoG base pair by preventing either 8-oxoG or the incoming adenine base from flipping into the *syn* conformation (*11*, *16*−*19*). As expected, substitution of a conserved Tyr with residues having smaller side chains, i.e., Y390S in ϕ29pol and Y955C in human pol γ (*16*, *19*), led to a significant decrease in the level of discrimination against insertion of dAMP relative to dCMP opposite 8-oxoG, but these losses were primarily due to a reduction in the insertion efficiency of dCMP, a result in contrast with that of the Y567A mutant of RB69pol (Table 2). These results suggest that RB69pol uses the conserved Y567 residue to discriminate against insertion of dAMP opposite 8-oxoG in a manner different from those of other DNA polymerases, even with DNA polymerases from the same family (e.g., ϕ29pol). However, we cannot rule out the possibility that the substitution of a Tyr with different residues (Ser, Cys, and Ala) would contribute significantly to these very different kinetic outcomes. Studies are underway to determine the effect of different Y567 substitutions on the fidelity of the 8-oxoG bypass.

In summary, the data presented here show that the role(s) of each conserved NBP residue in enhancing or reducing dNMP insertion efficiencies is largely influenced by nearby residues in the NBP. In addition, interactions that are not usually considered to be important, i.e., Cα-H···O=C or Cα-H···N hydrogen bonds, can stabilize nascent base pairs in a fashion that leads to rapid phosphoryl transfer. This underscores the need to improve our understanding of how NBP residues interact with nascent base pairs as well as with each other.

NOTE ADDED AFTER ASAP PUBLICATION

After this paper was published ASAP April 22, 2010, 7,8-dihydroxy-8-oxoguanine was changed to 7,8-dihydro-8-oxoguanine throughout. The revised version was reposted May 11, 2010.

REFERENCES

1. Roberts, J. K., and Kunkel, T. A., Eds. (1996) DNA replication in eukaryotic cells: Concepts, enzymes and systems, Cold Spring Harbor Laboratory Press, Plainview, NY.
2. Kunkel, T. A., and Erie, D. A. (2005) DNA mismatch repair. *Annu. Rev. Biochem. 74*, 681–710.
3. Marnett, L. J. (2000) Oxyradicals and DNA damage. *Carcinogenesis 21*, 361–370.
4. Hainaut, P., Hernandez, T., Robinson, A., Rodriguez-Tome, P., Flores, T., Hollstein, M., Harris, C. C., and Montesano, R. (1998) IARC Database of p53 gene mutations in human tumors and cell lines: Updated compilation, revised formats and new visualisation tools. *Nucleic Acids Res. 26*, 205–213.
5. Lindahl, T. (1993) Instability and decay of the primary structure of DNA. *Nature 362*, 709–715.
6. Shibutani, S., Takeshita, M., and Grollman, A. P. (1991) Insertion of specific bases during DNA synthesis past the oxidation-damaged base 8-oxodG. *Nature 349*, 431–434.
7. Sekiguchi, M., and Tsuzuki, T. (2002) Oxidative nucleotide damage: Consequences and prevention. *Oncogene 21*, 8895–8904.
8. Hsu, G. W., Ober, M., Carell, T., and Beese, L. S. (2004) Error-prone replication of oxidatively damaged DNA by a high-fidelity DNA polymerase. *Nature 431*, 217–221.
9. Lowe, L. G., and Guengerich, F. P. (1996) Steady-state and pre-steady-state kinetic analysis of dNTP insertion opposite 8-oxo-7,8-dihydroguanine by *Escherichia coli* polymerases I exo- and II exo. *Biochemistry 35*, 9840–9849.
10. Furge, L. L., and Guengerich, F. P. (1997) Analysis of nucleotide insertion and extension at 8-oxo-7,8-dihydroguanine by replicative T7 polymerase exo- and human immunodeficiency virus-1 reverse transcriptase using steady-state and pre-steady-state kinetics. *Biochemistry 36*, 6475–6487.
11. Brieba, L. G., Eichman, B. F., Kokoska, R. J., Doublie, S., Kunkel, T. A., and Ellenberger, T. (2004) Structural basis for the dual coding potential of 8-oxoguanosine by a high-fidelity DNA polymerase. *EMBO J. 23*, 3452–3461.
12. Brieba, L. G., Kokoska, R. J., Bebenek, K., Kunkel, T. A., and Ellenberger, T. (2005) A lysine residue in the fingers subdomain of T7 DNA polymerase modulates the miscoding potential of 8-oxo-7, 8-dihydroguanosine. *Structure 13*, 1653–1659.
13. Patro, J. N., Urban, M., and Kuchta, R. D. (2009) Interaction of human DNA polymerase α and DNA polymerase I from *Bacillus stearothermophilus* with hypoxanthine and 8-oxoguanine nucleotides. *Biochemistry 48*, 8271–8278.
14. Einolf, H. J., and Guengerich, F. P. (2001) Fidelity of nucleotide insertion at 8-oxo-7,8-dihydroguanine by mammalian DNA polymerase δ. Steady-state and pre-steady-state kinetic analysis. *J. Biol. Chem. 276*, 3764–3771.
15. Freisinger, E., Grollman, A. P., Miller, H., and Kisker, C. (2004) Lesion (in)tolerance reveals insights into DNA replication fidelity. *EMBO J. 23*, 1494–1505.
16. de Vega, M., and Salas, M. (2007) A highly conserved tyrosine residue of family B DNA polymerases contributes to dictate translesion synthesis past 8-oxo-7,8-dihydro-2′-deoxyguanosine. *Nucleic Acids Res. 35*, 5096–5107.
17. Wang, Y., and Schlick, T. (2007) Distinct energetics and closing pathways for DNA polymerase β with 8-oxoG template and different incoming nucleotides. *BMC Struct. Biol. 7*, 7.
18. Krahn, J. M., Beard, W. A., Miller, H., Grollman, A. P., and Wilson, S. H. (2003) Structure of DNA polymerase β with the mutagenic DNA lesion 8-oxodeoxyguanine reveals structural insights into its coding potential. *Structure 11*, 121–127.
19. Graziewicz, M. A., Bienstock, R. J., and Copeland, W. C. (2007) The DNA polymerase γ Y955C disease variant associated with PEO and parkinsonism mediates the incorporation and translesion synthesis opposite 7,8-dihydro-8-oxo-2′-deoxyguanosine. *Hum. Mol. Genet. 16*, 2729–2739.
20. Franklin, M. C., Wang, J., and Steitz, T. A. (2001) Structure of the replicating complex of a pol α family DNA polymerase. *Cell 105*, 657–667.
21. Zhang, H., Rhee, C., Bebenek, A., Drake, J. W., Wang, J., and Konigsberg, W. (2006) The L561A substitution in the nascent base-pair binding pocket of RB69 DNA polymerase reduces base discrimination. *Biochemistry 45*, 2211–2220.
22. Kuchta, R. D., Mizrahi, V., Benkovic, P. A., Johnson, K. A., and Benkovic, S. J. (1987) Kinetic mechanism of DNA polymerase I (Klenow). *Biochemistry 26*, 8410–8417.
23. Maniatis, T., Fritsch, E. F., and Sambrook, J. (1982) Molecular Cloning: A Laboratory Manual, Cold Spring Harbor Laboratory Press, Plainview, NY.
24. Zhang, H., Beckman, J., Wang, J., and Konigsberg, W. (2009) RB69 DNA polymerase mutants with expanded nascent base-pair-binding pockets are highly efficient but have reduced base selectivity. *Biochemistry 48*, 6940–6950.
25. Hanes, J. W., Thal, D. M., and Johnson, K. A. (2006) Incorporation and replication of 8-oxo-deoxyguanosine by the human mitochondrial DNA polymerase. *J. Biol. Chem. 281*, 36241–36248.
26. Hanes, J. W., and Johnson, K. A. (2007) A novel mechanism of selectivity against AZT by the human mitochondrial DNA polymerase. *Nucleic Acids Res. 35*, 6973–6983.
27. Otwinowski, Z., and Minor, W. (1997) Processing of X-ray diffraction data collected in oscillation mode. In Methods in Enzymology (Carter, C. W., and Sweet, R. M., Eds.) pp 307−326, Academic Press, San Diego.
28. Navaza, J. (1994) AMoRE: An automated package for molecular replacement. *Acta Crystallogr. A50*, 157–163.
29. Murshudov, G. N., Vagin, A. A., and Dodson, E. J. (1997) Refinement of macromolecular structures by the maximum-likelihood method. *Acta Crystallogr. D53*, 240–255.

30. Emsley, P., and Cowtan, K. (2004) Coot: Model-building tools for molecular graphics. *Acta Crystallogr. D60*, 2126–2132.
31. Carson, M. (1991) Ribbons 2.0. *J. Appl. Crystallogr. 24*, 958–961.
32. Bertram, J. G., Oertell, K., Petruska, J., and Goodman, M. F. (2010) DNA polymerase fidelity: Comparing direct competition of right and wrong dNTP substrates with steady state and pre-steady state kinetics. *Biochemistry 49*, 20–28.
33. Tsai, Y. C., and Johnson, K. A. (2006) A new paradigm for DNA polymerase specificity. *Biochemistry 45*, 9675–9687.
34. Senes, A., Ubarretxena-Belandia, I., and Engelman, D. M. (2001) The Cα-H···O hydrogen bond: A determinant of stability and specificity in transmembrane helix interactions. *Proc. Natl. Acad. Sci. U.S.A. 98*, 9056–9061.
35. Malins, D. C., and Haimanot, R. (1991) Major alterations in the nucleotide structure of DNA in cancer of the female breast. *Cancer Res. 51*, 5430–5432.
36. Degan, P., Shigenaga, M. K., Park, E. M., Alperin, P. E., and Ames, B. N. (1991) Immunoaffinity isolation of urinary 8-hydroxy-2′-deoxyguanosine and 8-hydroxyguanine and quantitation of 8-hydroxy-2′-deoxyguanosine in DNA by polyclonal antibodies. *Carcinogenesis 12*, 865–871.
37. David, S. S., O'Shea, V. L., and Kundu, S. (2007) Base-excision repair of oxidative DNA damage. *Nature 447*, 941–950.
38. McAuley-Hecht, K. E., Leonard, G. A., Gibson, N. J., Thomson, J. B., Watson, W. P., Hunter, W. N., and Brown, T. (1994) Crystal structure of a DNA duplex containing 8-hydroxydeoxyguanine-adenine base pairs. *Biochemistry 33*, 10266–10270.
39. Kouchakdjian, M., Bodepudi, V., Shibutani, S., Eisenberg, M., Johnson, F., Grollman, A. P., and Patel, D. J. (1991) NMR structural studies of the ionizing radiation adduct 7-hydro-8-oxodeoxyguanosine (8-oxo-7H-dG) opposite deoxyadenosine in a DNA duplex. 8-Oxo-7H-dG(syn)·dA(anti) alignment at lesion site. *Biochemistry 30*, 1403–1412.
40. Lipscomb, L. A., Peek, M. E., Morningstar, M. L., Verghis, S. M., Miller, E. M., Rich, A., Essigmann, J. M., and Williams, L. D. (1995) X-ray structure of a DNA decamer containing 7,8-dihydro-8-oxoguanine. *Proc. Natl. Acad. Sci. U.S.A. 92*, 719–723.
41. Yang, G., Wang, J., and Konigsberg, W. (2005) Base selectivity is impaired by mutants that perturb hydrogen bonding networks in the RB69 DNA polymerase active site. *Biochemistry 44*, 3338–3346.
42. Vargas, R., Garza, J., Dixon, D. A., and Hay, B. P. (2000) How strong is the Cα-H···O=C hydrogen bond? *J. Am. Chem. Soc. 122*, 4750–4755.
43. Scheiner, S., Kar, T., and Gu, Y. (2001) Strength of the Cα-H···O hydrogen bond of amino acid residues. *J. Biol. Chem. 276*, 9832–9837.
44. Zang, H., Irimia, A., Choi, J. Y., Angel, K. C., Loukachevitch, L. V., Egli, M., and Guengerich, F. P. (2006) Efficient and high fidelity incorporation of dCTP opposite 7,8-dihydro-8-oxodeoxyguanosine by *Sulfolobus solfataricus* DNA polymerase Dpo4. *J. Biol. Chem. 281*, 2358–2372.
45. Haracska, L., Yu, S. L., Johnson, R. E., Prakash, L., and Prakash, S. (2000) Efficient and accurate replication in the presence of 7,8-dihydro-8-oxoguanine by DNA polymerase *η*. *Nat. Genet. 25*, 458–461.
46. Wang, T. S., Wong, S. W., and Korn, D. (1989) Human DNA polymerase α: Predicted functional domains and relationships with viral DNA polymerases. *FASEB J. 3*, 14–21.
47. Saturno, J., Lazaro, J. M., Esteban, F. J., Blanco, L., and Salas, M. (1997) *ϕ*29 DNA polymerase residue Lys383, invariant at motif B of DNA-dependent polymerases, is involved in dNTP binding. *J. Mol. Biol. 269*, 313–325.